PHYSICAL REVIEW A **86**, 020701(R) (2012)

Shape resonance spectra of lignin subunits

Eliane M. de Oliveira,[1] Sergio d'A. Sanchez,[2] Márcio H. F. Bettega,[2] Alexandra P. P. Natalense,[1]
Marco A. P. Lima,[1,3] and Márcio T. do N. Varella[4]

[1]*Laboratório Nacional de Ciência e Tecnologia do Bioetanol (CTBE/CNPEM), CP 6170, 13083-970, Campinas, São Paulo, Brazil*
[2]*Departamento de Física, Universidade Federal do Paraná, CP 19044, 81531-990, Curitiba, Paraná, Brazil*
[3]*Instituto de Física "Gleb Wataghin", Universidade Estadual de Campinas, 13083-859, Campinas, São Paulo, Brazil*
[4]*Instituto de Física, Universidade de São Paulo, CP 66318, 05315-970, São Paulo, São Paulo, Brazil*

(Received 17 July 2012; published 20 August 2012)

We report integral cross sections for elastic electron scattering by the lignin subunits phenol, guaiacol, and *p*-coumaryl alcohol. Our calculations employed the Schwinger multichannel method with pseudopotentials and indicate three to four π^* shape resonances for each of these systems, suggesting that low-energy electrons could efficiently transfer energy into the lignin matrix. We also discuss dissociation mechanisms based on the calculated cross sections, available experimental data, virtual orbital analysis, and the knowledge on electron interactions with biomolecules. Our results point out a physical-chemical basis for electron-driven biomass delignification. The latter would be an essential step for efficient biofuel production from lignocellulosic materials.

DOI: 10.1103/PhysRevA.86.020701 PACS number(s): 34.80.Bm

Replacing fossil fuels for biofuels from renewable sources is a viable way to reduce greenhouse gas emissions. A successful example is the large-scale use of sugarcane ethanol to power light vehicles, especially after the development of flex-fuel engines that can run on any mixture of gasoline and ethanol [1]. A major goal to optimize biofuel production, either ethanol [2] or butanol [3], would be the development of high-yield methods to obtain fermentable sugars from lignocellulosic biomass, e.g., leaves, straw, and bagasse. Even though the cellulose basic unit is a fermentable sugar (β-D-glucose), lignocellulose is a composite material resistant to chemical or enzymatic hydrolysis. A dense hydrogen bonding network stabilizes the cellulose crystals that pack into fibers (∼45% of lignocellulose content), which are tightly embedded within hemicellulose (∼30% content) and lignin (∼25% content) [4]. Two key aspects regarding the biofuel industry would thus be biomass pretreatment technologies, namely bio- or physical-chemical processes that can improve the efficiency of subsequent hydrolysis, and the biorefinery concept, i.e., using the feedstock to produce high-value chemicals [5–7] along with biofuels.

Several pretreatment strategies have been proposed to expose cellulose chains, such as steam explosion, alkaline hydrolysis, and organosolv processes, among others [8]. Alternative technologies could be based on low-cost atmospheric-pressure plasmas [9–11] as the reactive species generated in discharge environments can increase the surface energy of cellulose and lignin films [10], and even allow for the real-time control of biomass delignification [11]. These promising results also draw attention to electron interactions with lignocellulose components. Free electrons can reach the substrate in atmospheric-pressure dielectric barrier discharge apparatuses [12], and low-pressure plasmas have long been applied in industrial processes, e.g., polymer surface modification [13]. Low-energy electrons ($\lesssim$20 eV) are known to induce dissociative processes that damage biomolecules either in gas or condensed phase [14,15]. The underlying mechanism is the formation of transient negative ions (resonances), since energy can efficiently be transferred into nuclear degrees of freedom upon electron attachment, leading to significant vibration excitation and dissociation.

Much of the current knowledge on electron-driven DNA damage was gained from studies on subunits, such as bases and sugars, as the attachment occurs in specific sites of the chain [14,16–18]. At low energies, the dominant mechanism for dissociative electron attachment (DEA) would involve shape resonances, i.e., anion states formed by adding an electron to the molecule ground state (into virtual orbitals) [19,20], specifically, the formation of long-lived π^* anions (attachment to π^* virtual orbitals) diabatically coupled to dissociative σ^* anions arising from antibonding virtual orbitals localized on polar bonds. From these facts, lignin would be expected to play an essential role in electron interactions with lignocellulose. While cellulose and hemicellulose are saturated polysaccharides, lignin is an aromatic copolymer that can give rise to long-lived π^* resonances. The lignin monomers (monolignols), namely, *p*-coumaryl alcohol, coniferyl alcohol, and sinapyl alcohol, are derived from phenol and differ in the degree of methoxylation, such that polar σ_{OH} and σ_{CO} bonds are also abundant.

This Rapid Communication surveys the low-energy shape resonance spectra of the lignin components phenol, guaiacol, and *p*-coumaryl alcohol (shown in Fig. 1), as obtained from elastic electron scattering cross sections. Based on well-known results for biomolecules, these subunits would be expected to provide essential information on electron-induced damage. Results for other lignin monomers, to be published elsewhere, also indicate that relevant aspects of the collision dynamics can be learned from the systems addressed here. The reported results provide insight into fundamental electron-transfer processes that might be of help for biomass delignification, a key pretreatment step that can yield value-added chemicals [6], and they will hopefully motivate other groups to further investigate electron interactions with lignocellulose.

Integral cross sections (ICSs) were obtained with the parallel version [21] of the Schwinger multichannel method with pseudopotentials (SMCPP) [22]. This variational approach to the T-matrix was discussed in detail elsewhere [21,22] and relies on a discrete trial set to expand the scattering state. The present calculations were performed in two approximations, namely, static-exchange (SE) and static-exchange plus

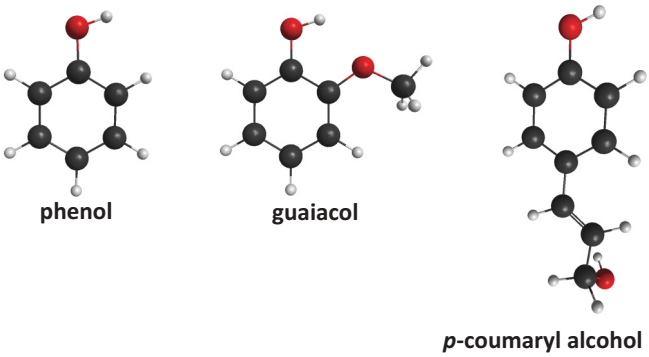

FIG. 1. (Color online) Structure of phenol, guaiacol, and *p*-coumaryl alcohol. Oxygen, carbon, and hydrogen atoms are shown in red (gray), black, and white, respectively.

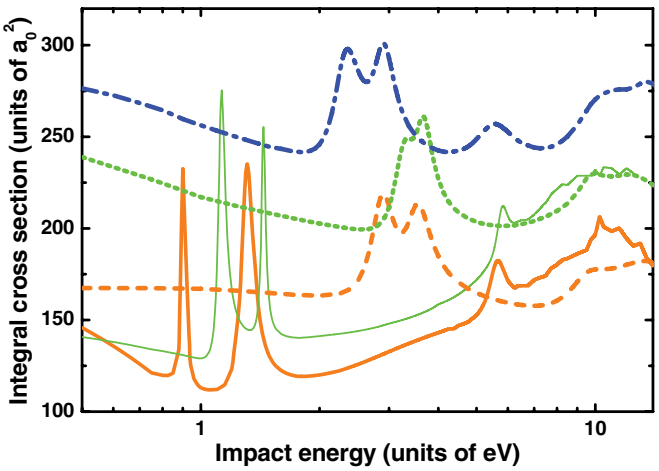

FIG. 2. (Color online) Integral cross sections for elastic electron scattering by lignin components. Results for phenol are shown in orange (gray), where the SE calculation is the dashed line and the SEP calculation is the thick solid line. Results for guaiacol are shown in green (light gray), where the SE calculation is the dotted line and the SEP calculation is the thin solid line. The SE calculation for *p*-coumaryl alcohol is the dotted-dashed line, shown in blue (dark gray).

polarization (SEP). In the former, the trial basis comprises antisymmetric $(N+1)$-electron configuration state functions (CSFs) of the form $|\Phi_0\rangle \otimes |\phi_j\rangle$, where $|\Phi_0\rangle$ is the N-electron target ground state and $|\phi_j\rangle$ is a scattering orbital. To account for correlation-polarization effects, the SEP trial basis is augmented with CSFs given by $|\Phi_\alpha\rangle \otimes |\phi_j\rangle$, where $|\Phi_\alpha\rangle$ is a singly excited virtual state of the target. In all calculations, the ground states (Φ_0) were described at the Hartree-Fock (HF) level employing Cartesian Gaussian basis sets given in the Supplemental Material (SM) [23]. For both the scattering orbitals set $\{\phi_j\}$ and the particle orbitals set (excited target states), we employed modified virtual orbitals (MVOs) obtained from Fock operators with charge +4. The ground-state structures shown in Fig. 1 were optimized with density functional theory employing the Becke three-parameter Lee-Yang-Parr (B3LYP) functional and the double-zeta valence DZV++$(2d,1p)$ basis set as implemented in the GAMESS package [24]. Though the target molecules are polar, the results were not corrected to account for the long-ranged dipole potential, since the latter should not give rise to shape resonances. Based on previous applications to several biomolecules, the methodology described above would be expected to accurately describe narrow resonances arising from π^* orbitals.

Phenol and guaiacol molecules have C_s symmetry. To account for polarization in the A'' component, we employed all symmetry-preserving single excitations out of the valence orbitals, with both singlet and triplet spin couplings, and the lowest three MVOs as scattering orbitals. This procedure would be expected to accurately describe the low-lying π^* resonances, as discussed in Ref. [25], where the number of scattering orbitals was based on the three π^* states obtained in the SE approximation for both molecules (see below). For the A' component, with a large background and no narrow resonances, we employed the lowest 40 MVOs as both scattering and particle orbitals to compromise between accuracy and computational effort. In SEP calculations, the variational space comprised 15 535 (14 484) CSFs in the A' (A'') symmetry for phenol, and 20 572 (24 037) for guaiacol. The SE and SEP results for phenol are shown in Fig. 2. By inspecting the symmetry decomposition of the ICS, we assigned three π^* resonances at 2.91, 3.57, and 9.72 eV. Polarization effects shift the peak positions to 0.91, 1.33, and 5.66 eV, respectively (the higher-lying structures are pseudoresonances that arise because electronic states that should be open were treated as closed channels). The two lowest π^* anion states are expected to have shape resonance character, while the highest-lying one would be an admixture of shape and core-excited anion states [26]. As shown in Table I, for the two shape resonances we find the expected good agreement ($\lesssim$0.4 eV error) with experimental assignments obtained from electron transmission spectroscopy (ETS) [27] and DEA cross sections [28]. The larger error for the third anion state is not surprising, since electronic excitation channels were not accounted for. Though a broad and low-lying resonance with σ^*_{OH} character would in principle be expected, we found no clear signature of such a state. As discussed elsewhere [21], this assignment would be difficult in view of the *s*-wave contribution, the large background, and even the coupling to virtual or dipole-supported states. Inspection of the lowest unoccupied molecular orbitals (LUMOs) obtained with the compact 6-31G(*d*) basis set, a procedure routinely employed in ETS assignments [29], suggests that a σ^*_{OH} resonance would indeed exist (this is also supported by DEA data [28]). Figure 3 shows the LUMO (π_1^*) and LUMO+1 (π_2^*) of phenol,

TABLE I. π^* resonance peak positions (in units of eV) obtained for phenol, guaiacol, and *p*-coumaryl alcohol in the SE and SEP approximations.

Phenol			Guaiacol		*p*-coumaryl
SE	SEP	Experiment	SE	SEP	SE
2.91	0.91	1.01[a]	3.32	1.13	2.36
3.57	1.33	1.73[a] (1.5[b])	3.66	1.44	2.89
					5.57
9.72	5.66	4.92[a] (5.1[b])	9.92	5.84	10.0

[a]Experimental assignments from Ref. [27].
[b]Experimental assignments from Ref. [28].

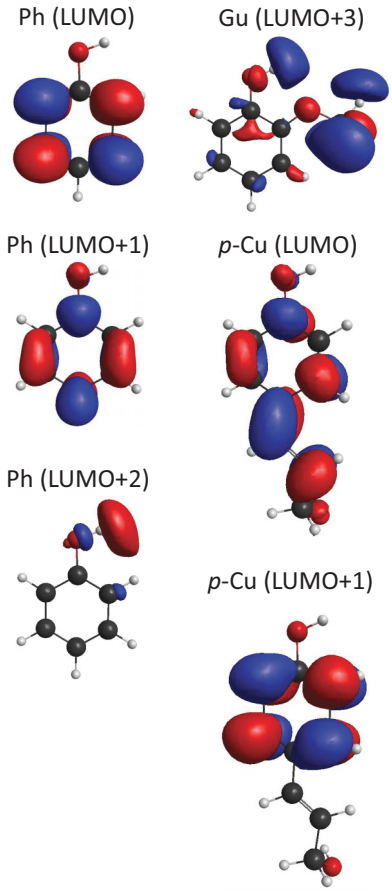

FIG. 3. (Color online) Virtual orbitals of the lignin components phenol (Ph), guaiacol (Gu), and *p*-coumaryl alcohol (*p*-Cu). The plots were generated with MACMOLPLT [30].

related to the lowest π^* shape resonances, along with the LUMO+2 (LUMO in A' symmetry) having σ^*_{OH} character. The ICS and VO plots suggest a reaction mechanism involving the π_2^* resonance and the σ^*_{OH} anion. Electron attachment to the π_2^* orbital would favor symmetry-breaking vibrations (to relieve the antibonding character), and the significant probability amplitudes around the C–O bond would allow for σ^*_{OH}-π_2^* coupling, thus giving rise to vibrational excitation and dissociation along the polar bond (hydrogen elimination). This reasoning is in qualitative agreement with DEA data [28], as a prominent peak arising from the $[M–H]^-$ anion (M denotes the parent molecule) is observed around 1.3–1.5 eV, along with the vibrational progression of the ν_{OH} mode. Though dissociation following attachment to the π_1^* orbital would not be expected, in view of the DEA threshold and the orbital density, significant vibrational excitation could arise from this anion state. It would be difficult to infer reaction pathways related to the third π^* resonance as electronic excitation would be expected to play a role.

p-coumaryl alcohol is obtained from phenol upon hydrogen substitution by the hydroxy-propenyl group ($-CH{=}CH_2{-}CH_2OH$) at the *para* position with respect to the hydroxyl group, and further methoxylation at the *ortho* positions gives rise to the other monolignols, coniferyl alcohol, and sinapyl alcohol. To survey the influence of the methoxyl and hydroxy-propenyl groups, we obtained the resonance spectra of guaiacol and *p*-coumaryl alcohol. The ICS of the former, calculated at the SE and SEP approximations, is shown in Fig. 2. Methoxylation does not significantly affect the π^* resonances, as expected. Guaiacol also displays three anion states in the A'' symmetry, lying slightly above those of phenol (see Table I). As discussed above, clear signatures of σ^* anion states would not be expected in the A' symmetry, and no electron-impact experimental data is available for guaiacol, to our knowledge. We thus inspected the A' LUMOs, also obtained with the 6-31G(d) basis set, finding that several orbitals would have significant probability on the hydroxyl and methoxyl moieties. For example, Fig. 3 shows the LUMO+1 orbital in the A' symmetry (LUMO+3 globally). Though we cannot come to a final conclusion only based on the VO analysis, the guaiacol orbital plots (see also the SM) suggest mechanisms for OH and CO bonds breakage arising from electron attachment to π^* orbitals, most likely the π_2^* resonance around 1.44 eV (see Table I). Even if the anion states could not give rise to DEA, vibrational excitation would surely take place, where $\pi^*_{1,2}$ resonance energies are similar to the excitation energy of singlet oxygen (1 eV), one of the main reactive species in atmospheric-pressure plasmas.

The SE approximation ICS of *p*-coumaryl alcohol is also shown in Fig. 2 (SEP calculations for this system would be very demanding). For phenol and guaiacol, the symmetry decomposition of SE cross sections indicates three structures in the A'' symmetry, namely, two low-lying π^* states below 4 eV and a higher-lying π^* anion ($\sim$9.8 eV), as well as a broad structure in the A' symmetry ($\sim$12 eV). Though this decomposition is not possible for *p*-coumaryl alcohol (C_1 group), the C=C bond in the propenyl group would be expected to give rise to an additional π^* state, so we assign three low-lying π^* resonances at 2.36, 2.89, and 5.57 eV, and a higher-lying one around 10 eV. In the latter case, we assumed that the lower of the two high-energy broad structures in the ICS, around 10 and 12 eV, would have a dominant π^* character. More interestingly the LUMO, shown in Fig. 3, suggests that the lowest π^* anion would be stabilized by conjugation. As inclusion of polarization shifted the lower-lying states of phenol and guaiacol by $\sim$2 eV, we would expect the lowest π^* resonance to be observed around $\lesssim$0.4 eV, such that dissociation could be induced at very low collision energies, as in DNA [19]. Finally, the LUMO+1 of *p*-coumaryl alcohol (shown in Fig. 3) is very similar to the LUMO of phenol, in consistency with the proximity of the corresponding resonance positions, lying around 2.9 eV in SE calculations.

In conclusion, lignin components have very rich π^* resonance spectra, such that low-energy electrons are expected to efficiently transfer energy into the lignin matrix. Though the assignment of low-lying σ^* anion states is difficult for the systems addressed here, the VO analysis (supported by experimental DEA data for phenol) indicate dissociation mechanisms similar to those established for DNA and its subunits. Altogether, the present results point out a physical-chemical basis for biomass delignification.

The authors acknowledge support from the Brazilian agencies FAPESP, CNPq, and Fundação Araucária. This work was

supported by the CNPq/NSF Cooperative Research Program and by the FAPESP Bioenergy Program (BIOEN 08/58034-0). The present calculations were performed at CENAPAD/SP, CTBE/CNPEM, IFGW/UNICAMP and LCPAD-UFPR. The authors thank Professor J. Amorim for helpful comments on atmospheric-pressure plasmas.

[1] At present, about 90% of light vehicles produced in Brazil are equipped with flex-fuel engines—see Ref. [2].
[2] R. C. de Cerqueira Leite, M. R. V. L. Leal, L. A. Cortez, W. M. Griffin, and M. I. G. Scandiffio, Energy **34**, 655 (2009).
[3] T. C. Ezeji, N. Qureshi, and H. P. Blaschek, Curr. Opin. Biotechnol. **18**, 220 (2007).
[4] P. H. F. Pereira, H. C. J. Voorwald, M. O. H. Cioffi, D. R. Mulinari, S. M. da Luz, and M. L. C. P. da Silva, BioRes. **6**, 2471 (2011).
[5] J. B. Binder and R. T. Raines, J. Am. Chem. Soc. **131**, 1979 (2009).
[6] D.-E. Kim and X. Pan, Ind. Eng. Chem. Res. **49**, 12156 (2010).
[7] M. Kosa and A. J. Ragauskas, Appl. Microbiol. Biot. **93**, 891 (2012).
[8] J. M. Taherzadeh and K. Keikhosro, Int. J. Mol. Sci. **9**, 1621 (2008).
[9] J. A. Souza-Corrêa, M. T. B. Pimenta, G. J. M. Rocha, E. O. Gomez, F. M. Squina, A. A. S. Curvelo, and J. Amorim, in *Plasmas for Environmental Issues*, Proceedings of the 2nd International Workshop at the 36th European Physical Society Conference on Plasma Physics, edited by E. Tatarova, V. Guerra, E. Benova, and A. Ricard (St. Kliment Ochridsky University, Sofia, Bulgaria, 2010), pp. 68–76.
[10] L. Klarhöfer, W. Viöl, and W. Maus-Friedrichs, Holzforschung **64**, 331 (2010).
[11] N. Schultz-Jensen, F. Leipold, H. Bindslev, and A. B. Thomsen, Appl. Biochem. Biotechnol. **163**, 558 (2010).
[12] From typical electron densities (10^{14} cm^{-3}) and velocities (10^{6} cm/s), the electronic flux on the substrate would be around 10^{8} cm^{-2} s^{-1}.
[13] For a review, see M. R. Wertheimera, A. C. Fozza, and A. Holländer, Nucl. Instrum. Methods B **151**, 65 (1999).
[14] For a review, see L. Sanche, Eur. Phys. J. D **35**, 367 (2005).
[15] C.-R. Wang, J. Nguyen, and Q.-B. Lu, J. Am. Chem. Soc. **131**, 11320 (2009).
[16] B. Boudaïffa, P. Cloutier, D. Hunting, M. A. Huels, and L. Sanche, Science **287**, 1658 (2000).
[17] M. A. Huels, B. Boudaïffa, P. Cloutier, D. Hunting, and L. Sanche, J. Am. Chem. Soc. **125**, 4467 (2002).
[18] X. Pan, P. Cloutier, D. Hunting, and L. Sanche, Phys. Rev. Lett. **90**, 208102 (2003).
[19] F. Martin, P. D. Burrow, Z. Cai, P. Cloutier, D. Hunting, and L. Sanche, Phys. Rev. Lett. **93**, 068101 (2004); K. Aflatooni, A. M. Scheer, and P. D. Burrow, J. Chem. Phys. **125**, 054301 (2006).
[20] I. Anusiewicz, M. Sobczyk, J. Berdys-Kochanska, P. Skurski, and J. Simons, J. Phys. Chem. A **109**, 484 (2005).
[21] J. S. dos Santos, R. F. da Costa, and M. T. do N. Varella, J. Chem. Phys. **136**, 084307 (2012).
[22] M. H. F. Bettega, L. G. Ferreira, and M. A. P. Lima, Phys. Rev. A **47**, 1111 (1993); R. F. da Costa, F. J. da Paixão, and M. A. P. Lima, J. Phys. B **37**, L129 (2004).
[23] See Supplemental Material at http://link.aps.org/supplemental/10.1103/PhysRevA.86.020701 for the Cartesian Gaussian basis sets emplyoed in bound-state and scattering calculations, and also for virtual orbital plots not shown here.
[24] M. W. Schmidt, K. K. Baldridge, J. A. Boatz, S. T. Elbert, M. S. Gordon, J. H. Jensen, S. Koseki, N. Matsunaga, K. A. Nguyen, S. J. Su, T. L. Windus, M. Dupuis, and J. A. Montgomery, J. Comput. Chem. **14**, 1347 (1993).
[25] C. Winstead and V. McKoy, Phys. Rev. A **57**, 3589 (1998).
[26] C. Winstead and V. McKoy, Phys. Rev. Lett. **98**, 113201 (2007).
[27] K. D. Jordan, J. A. Michejda, and P. D. Burrow, J. Am. Chem. Soc. **98**, 7189 (1976).
[28] R. V. Khatymov, M. V. Muftakhov, and V. A. Mazunov, Rapid Commun. Mass Spectrom. **17**, 2327 (2003).
[29] A. Modelli and P. W. Burrow, J. Phys. Chem. A **108**, 5721 (2004).
[30] B. M. Bode and M. S. Gordon, J. Mol. Graphics Modell. **16**, 133 (1998).